Available online at www.sciencedirect.com
ScienceDirect
Journal of Sound and Vibration 312 (2008) 461–475
JOURNAL OF SOUND AND VIBRATION
www.elsevier.com/locate/jsvi

# Application of a multivariable input–output subspace identification technique in structural analysis

Paulo Roberto Gardel Kurka[a,*], Heraldo N. Cambraia[b]

[a]Faculdade de Engenharia Mecânica, Universidade Estadual de Campinas, CEP 13083-860 Campinas, Sao Paulo, Brazil
[b]Departamento de Engenharia Mecânica, Universidade Federal do Paraná, Brazil

Received 28 September 2005; received in revised form 19 October 2006; accepted 11 July 2007
Available online 20 February 2008

**Abstract**

In this paper a multivariable subspace-based identification method is applied to experimental modal analysis. The method shows its efficiency in the identification of data which is contaminated by a great amount of external noise. Numerical simulation is used to present the main characteristics of the method and compare its performance against other techniques currently used in experimental modal analysis. The subspace identification method is also applied to data from a modal test of a practical engineering structure.


## 1. Introduction

The parametric identification of a multiple-input and multiple-output linear and time-invariant dynamical system is a problem of central importance in modal analysis. It is largely used in structural analysis, monitoring, model fitting or optimization design and control [1]. Multiple-input and multiple-output testing has many advantages when compared to single-input and single-output techniques, especially when dealing with larger structures. The force from multiple inputs allows a more uniform distribution of excitation energy throughout the structure, improving the accuracy of identified modal parameters and reducing the testing time.

The most common identification algorithms implemented in the time-domain use recursive linear difference equation models for describing the input–output relation, such as the auto-regressive with exogenous excitation (ARX) and auto-regressive moving average with exogenous excitation (ARMAX) [2]. The quality of identified parameters in those two approaches depends on the estimator adopted in the optimization process for calculating the fundamental matrix that comprises the model. The ARX model uses the well-known least-squares (LS) optimization criteria, which is very sensitive to the presence of noise in the data. The ARMAX model yields better accuracy when adopting iterative and nonlinear optimization schemes, at the expense of a very high computational effort, which limits its application to problems with a relatively small amount of data, which is not the case in multiple-input and multiple-output tests.

*Corresponding author. Tel.: +55 19 3521 3175; fax: +55 19 3289 3722.
*E-mail address:* kurka@fem.unicamp.br (P.R.G. Kurka).

0022-460X/$ - see front matter © 2007 Elsevier Ltd. All rights reserved.
doi:10.1016/j.jsv.2007.07.089

An alternative description for input–output relationship is the state-space model and a preferred solution for system identification is the use of subspace-based methods [3]. The main characteristic of such methods, for the noise-free situation, consists of the determination of poles using the shift-invariance property of the structured subspaces, defined by the columns or rows of data matrices obtained directly from the state-space formulation and input–output signals of the dynamic system. In the case of noise contaminated data, a filtered structured subspace is obtained by means of a low rank approximation matrix, using the singular value decomposition (SVD) technique.

The subspace scheme is able to perform a numerically reliable identification of parameters of a complex multivariable dynamical system, without the costly process of nonlinear search. The possibility of determining an approximate system order in the identification process, via inspection of the dominant singular value of the data matrix, is also an advantage of such a scheme.

Recent applications of the subspace technique show its ability to produce good parameter identification with relatively small computational effort in the case of output-only data information. The works by Peeters and De Roech [4], Hermans and Van Der Auweraer [5], Mevel et al. [6] and Abdelghani et al. [7], for example, show applications of output-only subspace methods ranging from civil damage detection to aircraft modal identification.

The current paper consists on the application of the parametric multiple-input and multiple-output input–output subspace identification method in experimental modal analysis from empirical input–output data. The method contributes in providing a robust model order determination based on a low rank approximation matrix using SVD, followed by natural frequencies and mode shapes estimation. The present method is distinct from output-only and input–output methods, cited above, since it uses an appropriated multi-input and single-output (MISO) realization that allows the determination of modal residues/mode shapes for multiple-input data.

Section 2 of the present paper derives the basic input–output signal relationship in a multivariable subspace approach. Section 3 addresses the details of finding practical system parameters in terms of poles (natural frequencies and modal damping) and mode shapes. Section 4 presents a numerical simulation which displays the technique's ability to identify parameters under the influence of noise contaminated data. Also in this section, the experimental testing of a truss structure is shown to further illustrate the applicability of the method.

## 2. Basic formulation

The response $\mathbf{y}(k)$ of a causal linear time-invariant system to a set of forces $\mathbf{u}(k)$ can be described as a finite-order discrete multivariable state-space model,

$$\begin{aligned} \mathbf{x}(k+1) &= \mathbf{A}\mathbf{x}(k) + \mathbf{B}\mathbf{u}(k), \\ \mathbf{y}(k) &= \mathbf{C}\mathbf{x}(k) + \mathbf{D}\mathbf{u}(k), \end{aligned} \tag{1}$$

where $\mathbf{x}(k)$ is the $n \times 1$ state-vector, $\mathbf{u}(k)$ is an $m \times 1$ input vector corresponding to $m$ inputs and $\mathbf{y}(k)$ is an $l \times 1$ output vector associated with $l$ response measurements. The quadruple of matrices $[\mathbf{A} \quad \mathbf{B} \quad \mathbf{C} \quad \mathbf{D}]$, with appropriate dimensions, contains the system dynamic characteristics.

The classical realization problem consists in finding a state-space representation $[\mathbf{A} \quad \mathbf{B} \quad \mathbf{C} \quad \mathbf{D}]$, such that the collection of impulse responses

$$\mathbf{h}(k) = \begin{cases} \mathbf{D} & (k = 0), \\ \mathbf{C}\mathbf{A}^{k-1}\mathbf{B} & (k > 0), \end{cases} \tag{2}$$

of the model matches the impulse response of the dynamical system to be modeled.

The term $\mathbf{h}(k)$ of Eq. (2), sometimes referred to as the Markov parameters [3], denotes the $l \times m$ matrix of impulse responses, where $h_{ij}(k)$ is a generic element of $\mathbf{h}(k)$ representing the response in output $i$ at time $k$ to a unit impulse applied to input $j$ at time 0.

The discussion here is limited to minimal state-space models, i.e., models for which the system order $n$ is minimal. A state-space model is considered minimal if there is no other realization of a degree that is lower than $n$ [3].

Input–output state-space time-domain realization methods attempt to find the system matrices **A**–**D**, from a given set of input and output data $\mathbf{u}(k)$ and $\mathbf{y}(k)$.

Sequences of $\mathbf{u}(k)$, $\mathbf{y}(k)$ and $\mathbf{x}(k)$ that satisfy Eq. (1) leads, after manipulation, to the important input–output matrix relationship:

$$\mathbf{Y}_h = \mathbf{\Gamma}_i \mathbf{X} + \mathbf{H}_t \mathbf{U}_h, \tag{3}$$

where $\mathbf{Y}_h$ and $\mathbf{U}_h$ are the $i$-block rows and $j$-columns Hankel matrices, containing output $\mathbf{y}(k)$ and input $\mathbf{u}(k)$ vectors of respective dimensions $il \times j$ and $im \times j$ as

$$\mathbf{Y}_h = \begin{bmatrix} \mathbf{y}(k) & \mathbf{y}(k+1) & \cdots & \mathbf{y}(k+j-1) \\ \mathbf{y}(k+1) & \mathbf{y}(k+2) & \cdots & \mathbf{y}(k+j) \\ \mathbf{y}(k+2) & \mathbf{y}(k+3) & \cdots & \mathbf{y}(k+j+1) \\ \vdots & \vdots & \ddots & \vdots \\ \mathbf{y}(k+i-1) & \mathbf{y}(k+i) & \cdots & \mathbf{y}(k+i+j-2) \end{bmatrix} \tag{4}$$

and

$$\mathbf{U}_h = \begin{bmatrix} \mathbf{u}(k) & \mathbf{u}(k+1) & \cdots & \mathbf{u}(k+j-1) \\ \mathbf{u}(k+1) & \mathbf{u}(k+2) & \cdots & \mathbf{u}(k+j) \\ \mathbf{u}(k+2) & \mathbf{u}(k+3) & \cdots & \mathbf{u}(k+j+1) \\ \vdots & \vdots & \ddots & \vdots \\ \mathbf{u}(k+i-1) & \mathbf{u}(k+i) & \cdots & \mathbf{u}(k+i+j-2) \end{bmatrix}. \tag{5}$$

**X** is a matrix of dimension $n \times j$, containing consecutive state-vectors and defined as

$$\mathbf{X} = \begin{bmatrix} \mathbf{x}(k) & \mathbf{x}(k+1) & \mathbf{x}(k+2) & \cdots & \mathbf{x}(k+j-1) \end{bmatrix}. \tag{6}$$

$\mathbf{\Gamma}_i$ is the $il \times n$ observability matrix formed by the state matrix **A** and the output influence matrix **C** as

$$\mathbf{\Gamma}_i = \begin{bmatrix} \mathbf{C} \\ \mathbf{CA} \\ \mathbf{CA}^2 \\ \vdots \\ \mathbf{CA}^{i-1} \end{bmatrix}. \tag{7}$$

$\mathbf{H}_t$ is a $il \times im$ lower triangular Toeplitz matrix formed from the first $i$ impulse responses as

$$\mathbf{H}_t = \begin{bmatrix} \mathbf{D} & \mathbf{0} & \mathbf{0} & \cdots & \mathbf{0} \\ \mathbf{CB} & \mathbf{D} & \mathbf{0} & \cdots & \mathbf{0} \\ \mathbf{CAB} & \mathbf{CB} & \mathbf{D} & \cdots & \mathbf{0} \\ \vdots & \vdots & \vdots & \ddots & \mathbf{0} \\ \mathbf{CA}^{i-2}\mathbf{B} & \mathbf{CA}^{i-3}\mathbf{B} & \mathbf{CA}^{i-4}\mathbf{B} & \cdots & \mathbf{D} \end{bmatrix}. \tag{8}$$

It can be seen from Eq. (7) that the observability matrix $\mathbf{\Gamma}_i$ has the following shift-invariant structure:

$$\mathbf{\Gamma}_i^{(2)} = \mathbf{\Gamma}_i^{(1)} \mathbf{A}, \tag{9}$$

where submatrices $\mathbf{\Gamma}_i^{(1)}$ and $\mathbf{\Gamma}_i^{(2)}$ are defined from $\mathbf{\Gamma}_i$ as

$$\mathbf{\Gamma}_i = \begin{bmatrix} \mathbf{\Gamma}_i^{(1)} \\ \mathbf{C}\mathbf{A}^{i-1} \end{bmatrix} = \begin{bmatrix} \mathbf{C} \\ \mathbf{\Gamma}_i^{(2)} \end{bmatrix}. \tag{10}$$

Assuming the realization to be of minimal order $n$, it follows that the observability matrix $\mathbf{\Gamma}_i$ is of full rank $n$, and the state matrix $\mathbf{A}$ can be estimated as

$$\mathbf{A} = \mathbf{\Gamma}_i^{(1)+}\mathbf{\Gamma}_i^{(2)}, \tag{11}$$

where the symbol "+" denotes the Moore–Penrose pseudo-inverse of matrix $\mathbf{\Gamma}_i^{(1)}$.

Basically, all the elements necessary to perform the state-space realization based on the input–output matrix relationship have been presented. The state matrix $\mathbf{A}$ is determined by solving Eq. (11) and matrix $\mathbf{C}$ can be obtained from the first block row of $\mathbf{\Gamma}_i$. The input influence matrices $\mathbf{B}$ and $\mathbf{D}$ can be calculated from the Toeplitz matrix $\mathbf{H}_i$. Appendix A presents a scheme to perform such a realization in practical terms. Several articles related to the state-space realization theory for input–output data can be found in the literature. The present formulation however is primarily based on Refs. [3,8,9].

The problem considered in this paper is related to the identification of modal parameters of a flexible structure given the input and output data measurements. The complex poles of the system are defined as [1]

$$\lambda_p = -\sigma_p + \mathrm{i}\omega_{dp}, \tag{12}$$

where $\sigma_p$ is the modal damping parameter, $\omega_{dp} = \omega_p\sqrt{1-\xi_p}$ is the damped natural frequency, $\xi_p$ is the viscous damping factor for mode $p$. The poles are calculated as

$$\lambda_p = \log(z_p)/\Delta t, \tag{13}$$

where log denotes natural logarithm, the term $z_p = \mathrm{e}^{\lambda_p \Delta t}$ represents the eigenvalues of the state matrix $\mathbf{A}$ and $\Delta t$ is the time sample adopted in the data acquisition process.

The modal residues associated with the poles $\lambda_p$ are defined as

$$r_{ij(p)} = \phi_{i(p)}\phi_{j(p)}, \tag{14}$$

where $r_{ij(p)}$ is the residue for mode $p$ at point $i$ due to an input at point $j$ and $\phi_{i(p)}$ is the $i$th element of the $p$th system mode shape. Residues estimation is discussed in the next section.

## 3. Modal parameters estimation

This section presents the poles and modal residues identification from the system realization based on the input–output data matrices $\mathbf{U}_h$ and $\mathbf{Y}_h$, respectively. In order to identify the system order $n$ and minimize the errors caused by the presence of noise in the estimation of matrix $\mathbf{A}$, a rank-reduction process is applied using the SVD. A starting high dimension (larger than $n$) input–output matrix equation allows for an appropriate column subspace representation of an extended observability matrix $\hat{\mathbf{\Gamma}}_i$, which is used to calculate matrix $\mathbf{A}$ as in Eq. (11). The residues are determined, using a particularly useful MISO realization scheme; in such a way that matrix $\mathbf{B}$ directly yields the residues of the system.

### 3.1. Pole identification

It is assumed that the input $\mathbf{u}(k)$ has sufficient energy to excite all modes of the system during the identification experiment, i.e., the system has persistent excitation [2]. In other words, the input $\mathbf{u}(k)$ contains at least $n/2$ harmonics with distinct frequencies that coincide with the natural frequencies of the system to be identified. Any white or colored input noise signal also satisfies this assumption. The consequent condition of persistent excitation is that matrix $\mathbf{U}_h$ from Eq. (5) is of full rank, $im$, considering that $j > (il, im)$. The SVD of matrix $\mathbf{U}_h$ yields,

$$\mathbf{U}_h = \mathbf{Q}\begin{bmatrix} \mathbf{S} & \mathbf{0}_{j_0} \end{bmatrix}\begin{bmatrix} \mathbf{V}_1^{\mathrm{T}} \\ \mathbf{V}_2^{\mathrm{T}} \end{bmatrix}, \tag{15}$$

where matrices $\mathbf{Q}$ and $\mathbf{S}$ have the same dimension $im \times im$. Matrix $\mathbf{0}_{j_0}$ has dimension $im \times j_0$ with $j_0 = j - im > im$. Matrices $\mathbf{V}_1$ and $\mathbf{V}_2$ have dimensions $j \times im$ and $j \times j_0$, respectively. Superscript T denotes matrix transposition.

It can be seen from Eq. (15) that matrix $\mathbf{Q}$ spans the column space of $\mathbf{U}_h$, whereas matrices $\mathbf{V}_1$ and $\mathbf{V}_2$ span, respectively, the row and null spaces of $\mathbf{U}_h$. Post multiplying Eq. (3) by $\mathbf{V}_2$ leads to

$$\mathbf{Y}_h\mathbf{V}_2 = \mathbf{\Gamma}_i\mathbf{X}\mathbf{V}_2 + \mathbf{H}_t\mathbf{U}_h\mathbf{V}_2 \tag{16}$$

which results in the following equation,

$$\mathbf{Y}_h\mathbf{V}_2 = \mathbf{\Gamma}_i\mathbf{X}\mathbf{V}_2, \tag{17}$$

where $\mathbf{Y}_h\mathbf{V}_2$ has dimension $il \times j_0$.

For the case of noise-free data, the rank of both matrices $\mathbf{\Gamma}_i$ and $\mathbf{V}_2^{\mathrm{T}}\mathbf{X}^{\mathrm{T}}$ is obviously $n$, which is also the order of the system. This enforces the product $\mathbf{Y}_h\mathbf{V}_2$ of Eq. (17) to be also order of $n$. Moreover, the $n$ columns of matrices $\mathbf{\Gamma}_i$ and $\mathbf{V}_2^{\mathrm{T}}\mathbf{X}^{\mathrm{T}}$ span, respectively, the column and row spaces of $\mathbf{Y}_h\mathbf{V}_2$, so that the column space of $\mathbf{Y}_h\mathbf{V}_2$ has the same shift-invariant structure as that of $\mathbf{\Gamma}_i$.

For the case where data is contaminated by noise, $\mathbf{Y}_h\mathbf{V}_2$ is full rank $il$, with $il > n$. However, a rank $n$ column space of $\mathbf{Y}_h\mathbf{V}_2$ can be calculated from the following SVD partition as

$$\mathbf{Y}_h\mathbf{V}_2 = \begin{bmatrix}\hat{\mathbf{Q}}_s & \hat{\mathbf{Q}}_n\end{bmatrix}\begin{bmatrix}\hat{\mathbf{S}}_s & \mathbf{0}\\ 0 & \hat{\mathbf{S}}_n\end{bmatrix}\begin{bmatrix}\hat{\mathbf{V}}_s^{\mathrm{T}}\\ \hat{\mathbf{V}}_n^{\mathrm{T}}\end{bmatrix} = \hat{\mathbf{Q}}_s\hat{\mathbf{S}}_s\hat{\mathbf{V}}_s^{\mathrm{T}} + \hat{\mathbf{Q}}_n\hat{\mathbf{S}}_n\hat{\mathbf{V}}_n^{\mathrm{T}}, \tag{18}$$

where matrices $\hat{\mathbf{Q}}_s$, $\hat{\mathbf{S}}_s$ and $\hat{\mathbf{V}}_s$ have dimensions $il \times n$, $n \times n$ and $j_0 \times n$, respectively. Obviously, in the absence of noise $\hat{\mathbf{S}}_n = 0$.

The $n$ columns of matrix $\hat{\mathbf{Q}}_s$ of dimension $il \times n$ span the column space of the $n$-order rank reduced matrix $\mathbf{Y}_h\mathbf{V}_2 \cong \hat{\mathbf{Q}}_s\hat{\mathbf{S}}_s\hat{\mathbf{V}}_s^{\mathrm{T}}$, recovered from a truncated SVD of $\mathbf{Y}_h\mathbf{V}_2$ using Eq. (18). Those columns contain also the $n$ principal left singular vectors corresponding to the $n$ principal singular values of the $n \times n$ diagonal matrix $\hat{\mathbf{S}}_s$.

In practice, the order $n$ of the dynamical system can be selected via inspection of the number of the most significant singular values of $\mathbf{Y}_h\mathbf{V}_2$. An estimate of the extended observability matrix $\mathbf{\Gamma}_i$, denoted by $\hat{\mathbf{\Gamma}}_i$, is then taken as,

$$\hat{\mathbf{\Gamma}}_i = \hat{\mathbf{Q}}_s \tag{19}$$

since the theoretical observability matrix $\mathbf{\Gamma}_i$ and the extended observability matrix $\hat{\mathbf{\Gamma}}_i = \hat{\mathbf{Q}}_s$ span the column space of the data matrix $\mathbf{Y}_h\mathbf{V}_2$, respectively, for the ideal free-noise and noise contaminated cases, for some $n$-order state-space realization.

The $n$ system's poles $\lambda_p$ are identified using Eqs. (9)–(13).

### 3.2. Residues and mode shapes estimation

Under the assumption of distinct system's poles, there are, in fact, an infinite number of state-space realizations of a system, as represented in Eq. (1). Equivalent representations can be obtained by using an invertible state-vector transformation $\mathbf{T}$ of dimension $n \times n$ to define a new state-vector $\bar{\mathbf{x}}(k) = \mathbf{T}\mathbf{x}(k)$, yielding an equivalent state-space model as

$$\begin{aligned}\bar{\mathbf{x}}(k+1) &= \mathbf{T}\mathbf{A}\mathbf{T}^{-1}\bar{\mathbf{x}}(k+1) + \mathbf{T}\mathbf{B}\mathbf{u}(k),\\ \mathbf{y}(k) &= \mathbf{C}\mathbf{T}^{-1}\bar{\mathbf{x}}(k) + \mathbf{D}\mathbf{u}(k)\end{aligned} \tag{20}$$

and producing an equivalent state-space realization given by

$$\begin{bmatrix}\bar{\mathbf{A}} = \mathbf{T}\mathbf{A}\mathbf{T}^{-1} & \bar{\mathbf{B}} = \mathbf{T}\mathbf{B} & \bar{\mathbf{C}} = \mathbf{C}\mathbf{T}^{-1} & \bar{\mathbf{D}} = \mathbf{D}\end{bmatrix}. \tag{21}$$

The eigenvalues of matrix $\bar{\mathbf{A}}$ remain invariant under this transformation $\mathbf{T}$ since $\mathbf{T}\mathbf{A}\mathbf{T}^{-1}$ is a similarity transformation [9].

In order to calculate the modal residues $r_{ij(p)}$, an appropriate realization, which is valid for the $m$ inputs and a single-output (MISO) case, is defined as

$$\begin{bmatrix} \mathbf{A}_d & \mathbf{B}_d \\ \mathbf{C}_d & \mathbf{D}_d \end{bmatrix} = \begin{bmatrix} z_1 & & & r_{i1(1)} & \cdots & r_{im(1)} \\ & \ddots & & \vdots & \ddots & \vdots \\ & & z_n & r_{i1(n)} & \cdots & r_{im(n)} \\ 1 & \cdots & 1 & d_1 & \cdots & d_m \end{bmatrix}, \tag{22}$$

where $\mathbf{A}_d = \mathbf{Z} = \mathrm{diag}\{z_1, \ldots, z_n\}$ of dimension $n \times n$ contains the $n$ parameters $z_p = \mathrm{e}^{\lambda_p \Delta t}$ and each column of matrix,

$$\mathbf{B}_d = \begin{bmatrix} r_{i1(1)} & \cdots & r_{im(1)} \\ \vdots & \ddots & \vdots \\ r_{i1(n)} & \cdots & r_{im(n)} \end{bmatrix} \tag{23}$$

of dimension $n \times m$ contains, directly, the modal residues of the impulse responses $h_{ij}(z)$'s for $i$th output point corresponding to the $j = 1, \ldots, m$ input points.

The application of input–output identification procedure presented in this paper produces a generic system realization given by $\begin{bmatrix} \mathbf{A} & \mathbf{B} & \mathbf{C} & \mathbf{D} \end{bmatrix}$. The particular realization given by Eq. (22) is obtained by applying a state-vector transformation $\mathbf{T}_d$, such that $\mathbf{A} = \mathbf{T}_d^{-1}\mathbf{Z}\mathbf{T}_d$. Moreover, it can be seen in Eq. (21) the matrices $\mathbf{B}$ and $\mathbf{B}_d$ are related by

$$\mathbf{B}_d = \mathbf{T}_d\mathbf{B}, \tag{24}$$

where the determination of matrix $\mathbf{B}$ and an appropriate state-vector transformation $\mathbf{T}_d$ are, respectively, described in Appendices A and B.

The modal residues $r_{ij(p)}$, for totality of all $m$ inputs and $l$ outputs (multiple-input and multiple-output), are calculated by applying sequentially the above MISO procedure for each measured output. This way, the process of finding matrix $\mathbf{B}$ is repeated $l$ times, yielding the matrices $\mathbf{B}^{(1)} \quad \mathbf{B}^{(2)} \quad \cdots \quad \mathbf{B}^{(l)}$ of dimension $n \times m$, associated with the $m$ inputs and a single output described above. The corresponding $\mathbf{B}_d$ matrix is calculated from Eq. (24) as

$$\mathbf{B}_d^i = \mathbf{T}_d\mathbf{B}^{(i)} = \begin{bmatrix} r_{i1(1)} & r_{i2(1)} & \cdots & r_{im(1)} \\ r_{i1(2)} & r_{i2(2)} & \cdots & r_{im(2)} \\ \vdots & \vdots & \ddots & \vdots \\ r_{i1(n)} & r_{i2(n)} & \cdots & r_{im(n)} \end{bmatrix}. \tag{25}$$

Finally, the mode shapes are determined using the equality $r_{ij(p)} = \phi_{i(p)}\phi_{j(p)}$, where $\phi_{i(p)}$ represents the $i$th element of the $p$th shape mode associated to the $p$th system pole $\lambda_p = -\sigma_p + \mathrm{i}\omega_{dp}$.

## 4. Results

This section presents the performance of the presented subspace realization method on both simulated and experimental data sets.

### 4.1. Numerical simulation

A multiple-input and multiple-output example, using computer simulated data sets for 2 inputs and 3 outputs, is shown in order to compare the performance of the subspace method with an auto-regressive with exogenous input (ARX) method [10]. The impulse response functions $h_{11}$, $h_{21}$, $h_{31}$, $h_{23}$ and $h_{33}$ of a typical (mass, spring and damping) system with three degrees of freedom are generated with poles and correspondent residues shown, respectively, in the fist column of Tables 1 and 2. The outputs $y_1$, $y_2$ and $y_3$ have been

Table 1
Identified poles

| Original poles | Subspace method | ARX |
|---|---|---|
| $\lambda_1 = -0.0196 + 6.6533i$ | −0.0199–6.6543i | −0.0231–6.6521i |
| $\lambda_2 = -0.0496 + 10.5300i$ | −0.0485–10.5297i | −0.0606–10.5246i |
| $\lambda_3 = -0.1307 + 16.2737i$ | −0.1230–16.2783i | −0.1856–16.2319i |
| $N_p = 550$, $\Delta t = 0.125$, $i = 20$, $j = 530$, NSR = 0.32 | | |

Table 2
Identified residues

| | Subspace method | ARX |
|---|---|---|
| *Original residue r11* | | |
| 1.4e−06−0.00012i | 0.0002−0.0001i | 0.0018−0.0001i |
| 4.6e−06−0.00046i | 0.0002−0.0046i | 0.0028−0.0054i |
| −1.3e−07 + 3.7e−06i | −0.0006 + 0.0009i | −0.0012 + 0.0041i |
| *Original residue r12* | | |
| 4.6e−06−0.0008i | 0.0004−0.0008i | 0.0015−0.0010i |
| 3.6e−06 + 0.0004i | 0.0003 + 0.0005i | 0.0020 + 0.0017i |
| 1.1e−06 + 5.8e−05i | 0.0003 + 0.0005i | 0.0000 + 0.0011i |
| *Original residue r13* | | |
| −3.1e−06−0.0005i | −0.0004−0.0003i | −0.0014−0.0012i |
| −4.6e−06 + 4.6e−04i | −0.0004 + 0.0024i | −0.0004 + 0.0029i |
| −1.6e−06−9.0e−05i | −0.0206−0.0006i | −0.0656−0.0010i |
| *Original residue r23* | | |
| −0.0000–0.0034i | −0.0002−0.0033i | −0.0029−0.0042i |
| −7.8e−07−4.1e−05i | −0.0002−0.0001i | −0.0030−0.0006i |
| −0.0000 + 0.0014i | −0.0000 + 0.0012i | −0.0011 + 0.0023i |
| *Original residue r33* | | |
| 0.0000–0.0022i | 0.0000−0.0021i | 0.0000−0.0019i |
| 9.3e−07−4.6e−005i | 0.0001−0.0002i | 0.0024−0.0032i |
| 0.0000–0.0022i | 0.0004−0.0022i | 0.0054−0.0048i |

calculated using the following discrete convolutions:

$$y_1(k) = \sum_{s=0}^{Np} h_{11}(s)u_1(k-s) + \sum_{s=0}^{Np} h_{13}(s)u_2(k-s),$$
$$y_2(k) = \sum_{s=0}^{Np} h_{21}(s)u_1(k-s) + \sum_{s=0}^{Np} h_{23}(s)u_2(k-s),$$
$$y_3(k) = \sum_{s=0}^{Np} h_{31}(s)u_1(k-s) + \sum_{s=0}^{Np} h_{33}(s)u_2(k-s), \quad (26)$$

where $u_1$ and $u_2$ are zero mean Gaussian inputs with amplitude 5. The discretization interval $\Delta t$ used in the simulation is 0.125 s. No input process noise is added, whereas white Gaussian noise with zero mean and noise to signal ratio (NSR) of approximately 0.30 is added to the outputs.

The identification techniques are applied to the input–output data set with a number of samples $N_p = 550$. Also, $i = 20$ and $j = N_p - i = 530$ are the assumed values to form the $i$-blocks rows and $j$-columns Hankel matrices $\mathbf{Y}_h$ and $\mathbf{U}_h$ from Eqs. (4) and (5), resulting in a $\mathbf{Y}_h\mathbf{V}_2$ matrix of dimension $60 \times 490$ according to

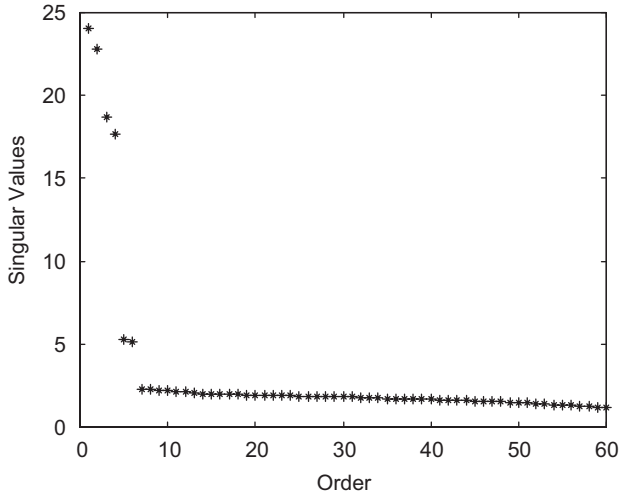


Fig. 1. Singular values of $\mathbf{Y}_h\mathbf{V}_2$.

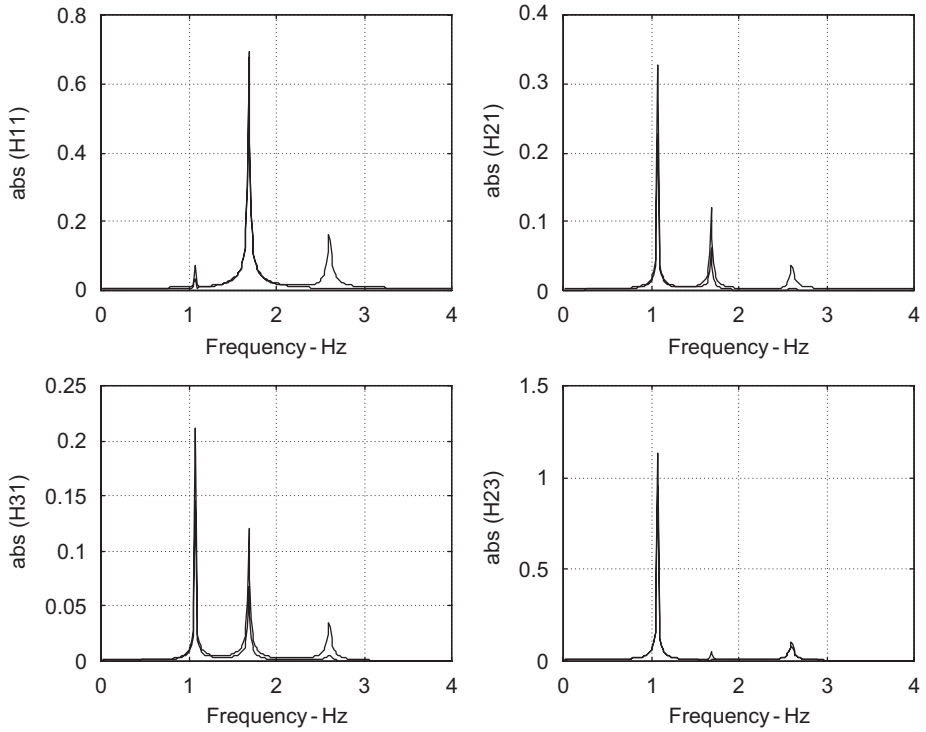


Fig. 2. Original and identified frequency response function magnitudes generated via the subspace method.

Eq. (17). The model order is identified as $n = 6$ by inspection of the principal singular values of matrix $\mathbf{Y}_h\mathbf{V}_2$ as shown in Fig. 1. Tables 1 and 2 show the identified poles and residues calculated by the presented method as compared to those obtained via the ARX, using the information of the identified system order, on both identification procedures. The comparison reveals better parameter estimations in the subspace method than those obtained via the ARX method. This is typical of the small sensibility to noise of the subspace method. Fig. 2 shows the comparison of the original and identified frequency response functions through the subspace method.

Two other problems associated with the application of the ARX method in modal analysis is the difficulty to identify the system order in the presence of computational poles as resulting in the analysis. In this example, it has to reach 6 true system poles within a total of 60 values obtained from the eigenvalues of the companion matrix calculated by means of an overestimated LS linear solution involving the data matrices [10].

### 4.2. Experimental results

This section presents the experimental modal identification analysis using the input–output subspace method presented in this paper. Two tests of a practical structure are considered, one for single-input and single-output data sets and another for data sets comprised of two simultaneous inputs and two outputs. The results of the identification consist of the determination of the natural frequencies and vibration mode shapes. The structure used in the experimental modal identification procedure is a free–free spatial truss with 28 measuring points, as shown in Fig. 3.

For the single-input and single-output test, the structure is excited with uncorrelated pseudo-random input signal by means of one electromagnetic shaker mounted at point 01. One simultaneous acceleration measurement is measured for each of the 28 measuring points, making a total of 28 sets of single-input and single-output tests, conducted at a sampling rate of 2500 Hz. The signals are filtered at a cut-off frequency of 1000 Hz. A number of $N_p = 800$ data samples are taken at each measuring point. The time-domain subspace-based identification method, presented in Section 3 above, is performed for each single-input and single-output testing ($m = 1$ and $l = 1$) with a Hankel input $\mathbf{Y}_h$ and output $\mathbf{U}_h$ block matrices of $i = 100$ rows and $j = N_p - i = 700$ columns, resulting in a $\mathbf{Y}_h\mathbf{V}_2$ matrix of dimension $100 \times 600$ according to Eq. (17).

The first stage in the subspace realization procedure consists in the determination of the minimum order of the model system. The singular values of $\mathbf{Y}_h\mathbf{V}_2$ are displayed in Fig. 4. According to the criteria based on the inspection of the principal singular values of $\mathbf{Y}_h\mathbf{V}_2$, the order used for the analysis is adopted as $n = 20$. The second stage of the method is the calculation of the extended observability matrix $\hat{\mathbf{\Gamma}}_i = \hat{\mathbf{Q}}_{s_n}$ from a rank $n$ reduced approximation of $\mathbf{Y}_h\mathbf{V}_2$, as shown in Eq. (18). The shift-invariant property of matrix $\hat{\mathbf{\Gamma}}_i$, of dimension $100 \times 20$, is used for the estimation of poles, according to Eq. (11). Finally, the modal residues are estimated using the procedure described in Section 3.2.

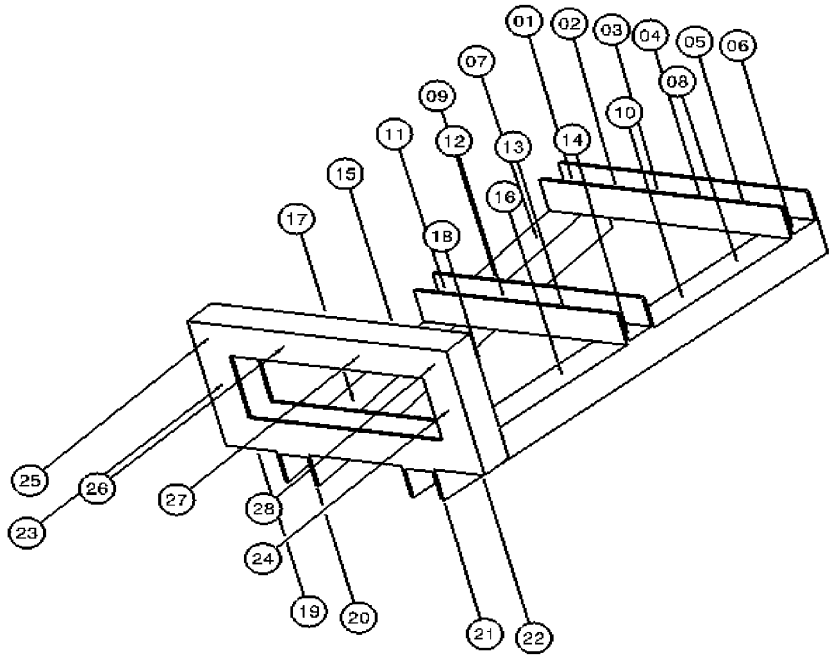


Fig. 3. The spatial truss.

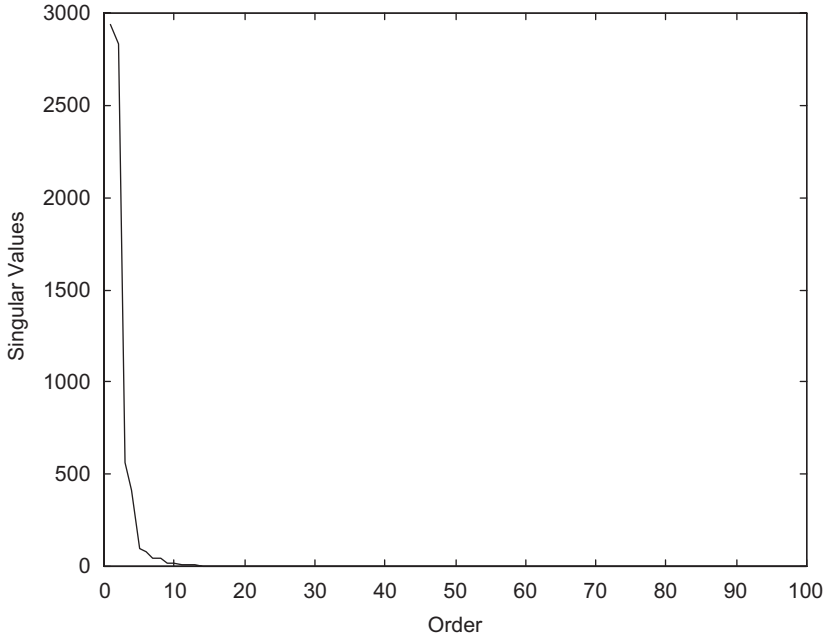


Fig. 4. Singular values of $\mathbf{Y}_h\mathbf{V}_2$.

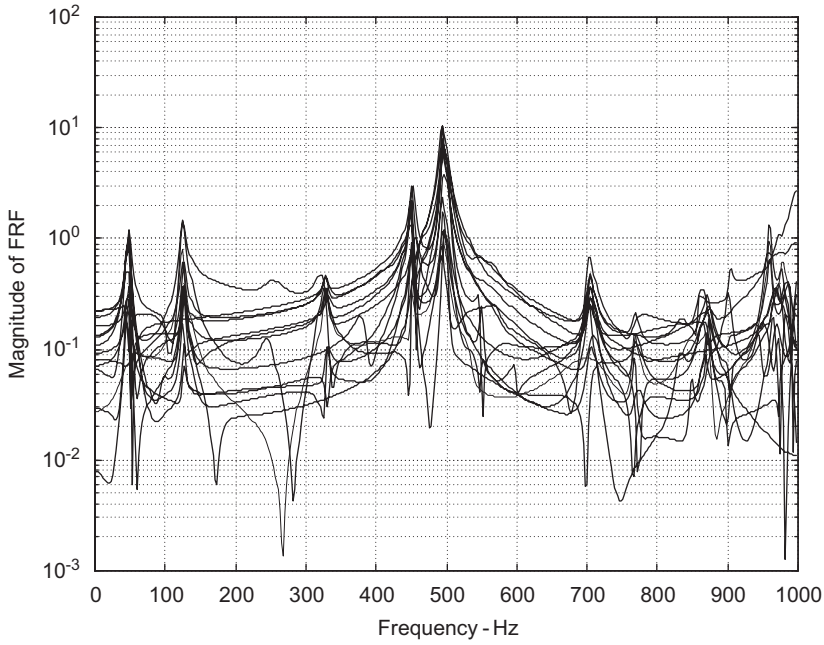


Fig. 5. Synthesized frequency response function magnitudes generated from identified modal parameters.

Typical synthesized acceleration frequency response function magnitudes are calculated using the identified poles and modal residues and are shown in Fig. 5. Fig. 6 shows the mean values of such synthesized frequency response function magnitudes. The measured natural frequencies are calculated as $\omega_p = \left|\mathrm{Im}\left(\lambda_p\right)\right|$. The location of the most relevant frequency response peaks in the synthesized mean frequency response function magnitude curve are shown in Table 3. The associated real modal deflections of complex mode shapes,

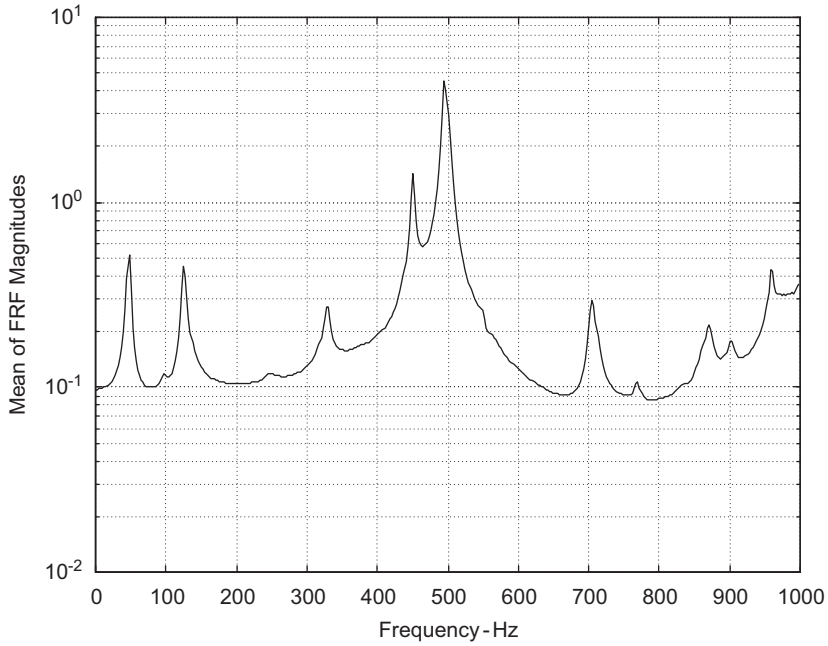


Fig. 6. Mean value of the magnitude of the synthesized frequency response functions for the single-input and single-output case.

Table 3
Identified natural frequencies

| Frequency (Hz) | | | | | | |
|---|---|---|---|---|---|---|
| 47.5 | 127.5 | 328.0 | 450.0 | 495.0 | 708.0 | 870.0 |

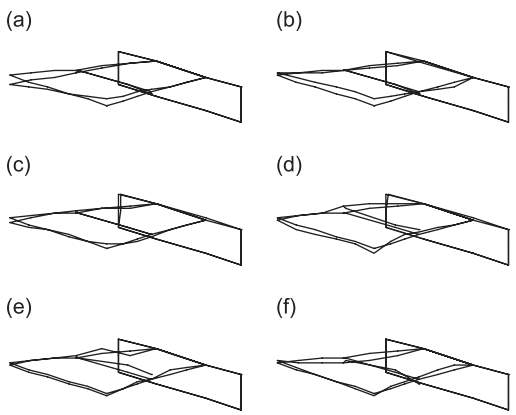


Fig. 7. Modes of vibration for single-input and single-output case corresponding to the following frequencies: (a) 47.5 Hz, (b) 127.5 Hz, (c) 328.0 Hz, (d) 450.0 Hz, (e) 495.0 Hz and (f) 708.0 Hz.

obtained using the modal residues by $r_{ij(p)} = \phi_{i(p)}\phi_{j(p)}$, are presented in Fig. 7. The real modal deflection is calculated as $\phi^r_{i(p)} = \text{abs}(\phi_{i(p)})\sin(\text{angle}(\phi_{i(p)}))$, where $p$ represents the associated index frequency [11].

A multiple-input and multiple-output experiment is made using the same truss structure excited by two shakers mounted at points 01 and 16, both using pseudo-random input. Two simultaneous acceleration measurements are taken for all 28 measuring points characterizing a total of 14 sets of two-input two-output

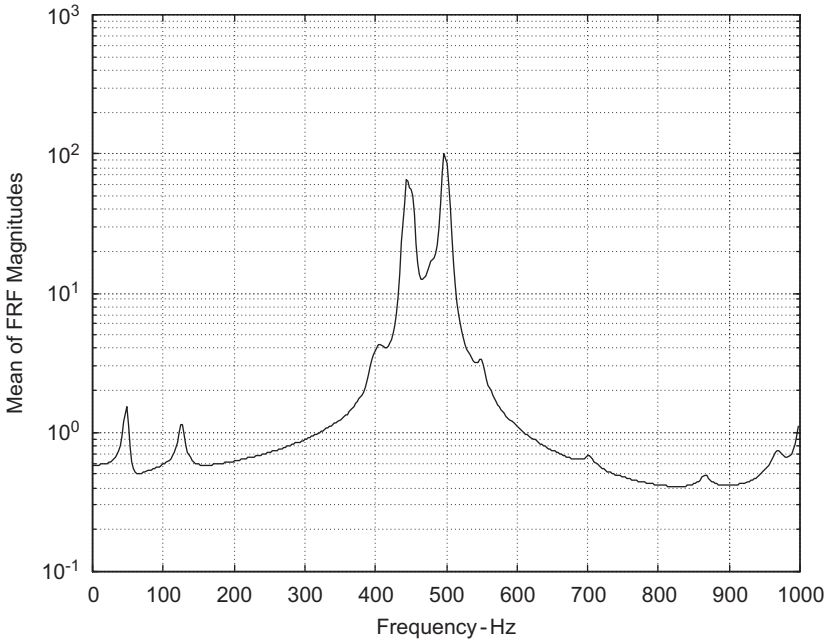


Fig. 8. Mean value of the magnitude of the synthesized frequency response functions for the multiple-input and multiple-output case.

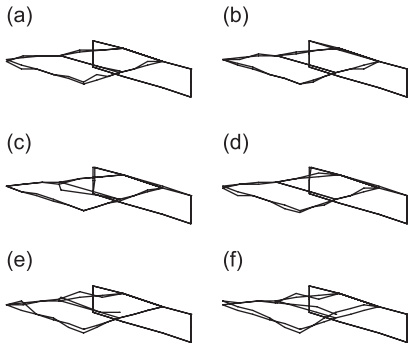


Fig. 9. Modes of vibration for multiple-input and multiple-output case corresponding to the following frequencies: (a) 47.5 Hz, (b) 127.5 Hz, (c) 328.0 Hz, (d) 450.0 Hz, (e) 495.0 Hz and (f) 708.0 Hz.

tests using the cut-off frequency of 1000 Hz and the number of time sample points as $N_p = 800$. The identification ($m = 2$ and $l = 2$) multiple-input and multiple-output procedure uses the Hankel input $\mathbf{Y}_h$ and output $\mathbf{U}_h$ block matrices with $i = 100$ rows and $j = N_p - i = 700$ columns, resulting in a $\mathbf{Y}_h\mathbf{V}_2$ matrix of dimension $200 \times 500$. The model order adopted in the test, after analysis of the singular values of $\mathbf{Y}_h\mathbf{V}_2$ is also $n = 20$. The dimension of matrix $\hat{\mathbf{\Gamma}}_i$ is now $200 \times 20$ from which the poles are estimated. Residues are calculated according to the procedure described in Section 3.2 by applying twice the MISO residue identifications for each measured output data set. The mean value of the magnitudes of the synthesized (frequency response functions) is shown in Fig. 8. The natural frequencies are approximately the same obtained from the single-input and single-output case and the correspondent mode shapes are presented in Fig. 9. It is noted that the identified natural frequencies have approximately the same values for both the single-input and single-output and multiple-input and multiple-output cases, whereas the vibrating mode shapes present some differences. The differences are gathered to be due to the fact that the truss being relatively small, the physical interaction of the two excitation shakers tends to slightly modify the shapes of vibration.

## 5. Conclusion

This paper presents the development and application of a multivariate subspace-based state-space formulation for modal parameter identification using input–output data. The technique, brought to the context of structural analysis, is grouped in the class of realization-based methods which are mostly used in electrical engineering applications. Another important contribution of the work is the formulation of residues derived directly from the system realization model. The ability to provide accurate modal parameters estimations with a lean computational performance and numerical efficiency makes the method attractive for both control and modal analysis applications.

## Acknowledgements

This work was supported by Coordenadoria de Aperfeiçoamento de Pessoal de Nível Superior—CAPES—Brazil. Project ref. 23075-960/99-23.

## Appendix A. Determination of matrices B and D

Matrices $\mathbf{B}$ and $\mathbf{D}$ are found through pre- and post-multiplication of Eq. (3) by quantities $\hat{\mathbf{Q}}_n^{\mathrm{T}}$ and $\mathbf{U}_h^{\mathrm{T}}$, respectively, from Eqs. (18) and (3). Considering the orthogonal property of $\hat{\mathbf{Q}}_s$ and $\hat{\mathbf{Q}}_n$ from Eq. (18), the following equality can be established:

$$\hat{\mathbf{Q}}_n^{\mathrm{T}}\mathbf{H}_t = \hat{\mathbf{Q}}_n^{\mathrm{T}}\mathbf{R}_{yu}\mathbf{R}_{uu}^{-1}, \tag{A.1}$$

where $\mathbf{R}_{yu} = \mathbf{Y}_h\mathbf{U}_h^{\mathrm{T}}$ is the $il \times im$ cross-correlation matrix of the input and output and $\mathbf{R}_{uu} = \mathbf{U}_h\mathbf{U}_h^{\mathrm{T}}$ is the $im \times im$ autocorrelation matrix of the input. Matrices $\mathbf{B}$ and $\mathbf{D}$ can be determined, after partitioning and rearranging of Eq. (A.1), using the standard LS techniques. One appropriate way of computing $\mathbf{B}$ and $\mathbf{D}$, can be found in Ref. [8] as

$$\begin{bmatrix}\mathbf{D}\\ \mathbf{B}\end{bmatrix} = \tilde{\mathbf{Q}}^{+}\tilde{\mathbf{R}}, \tag{A.2}$$

where the symbol $+$ denotes the Moore–Penrose pseudo-inverse of matrix $\tilde{\mathbf{Q}}$ to be defined below.

Matrices $\tilde{\mathbf{Q}}$ and $\tilde{\mathbf{R}}$ have dimensions $in_0 \times (l+n)$ and $in_0 \times m$, respectively, with $n_0 = il-n$ and are defined as

$$\tilde{\mathbf{Q}} = \begin{bmatrix} \hat{\mathbf{Q}}_n^{\mathrm{T}}(:,1:l) & \hat{\mathbf{Q}}_n^{\mathrm{T}}(:,l+1:li)\hat{\mathbf{Q}}_s(1:l(i-1),:) \\ \hat{\mathbf{Q}}_n^{\mathrm{T}}(:,l+1:2l) & \hat{\mathbf{Q}}_n^{\mathrm{T}}(:,2l+1:li)\hat{\mathbf{Q}}_s(1:l(i-2),:) \\ \hat{\mathbf{Q}}_n^{\mathrm{T}}(:,2l+1:3l) & \hat{\mathbf{Q}}_n^{\mathrm{T}}(:,3l+1:li)\hat{\mathbf{Q}}_s(1:l(i-3),:) \\ \vdots & \vdots \\ \hat{\mathbf{Q}}_n^{\mathrm{T}}(:,l(i-1)+1:li) & \mathbf{0}_{n_0\times n} \end{bmatrix} \tag{A.3}$$

and

$$\tilde{\mathbf{R}} = \begin{bmatrix} \mathbf{R}(:,1:m) \\ \mathbf{R}(:,m+1:2m) \\ \mathbf{R}(:,2m+1:3m) \\ \vdots \\ \mathbf{R}(:,m(i-1)+1:mi) \end{bmatrix}. \tag{A.4}$$

Matrix $\mathbf{R} = \hat{\mathbf{Q}}_n^{\mathrm{T}}\mathbf{R}_{yu}\mathbf{R}_{uu}^{-1}$ from the above equation represents the right-hand side of Eq. (A.1) and $\tilde{\mathbf{R}}$ is formed by partitions of $\mathbf{R}$. For the MISO identification case, to be used in Section 3 for the residues estimation, the

first row of matrix $\tilde{\mathbf{Q}}^{+}\tilde{\mathbf{R}}$ is matrix $\mathbf{D}$ in itself, whereas the last $n$ rows determine matrix $\mathbf{B}$. For more information about the estimation of matrices $\mathbf{B}$ and $\mathbf{D}$, see Ref. [8].

## Appendix B. Determination of the similarity transformation $\mathbf{T}_d$

In order to calculate a state-vector transformation to be used in the residue estimation process adopted here, it is convenient to introduce two important $i$-block rows and $j$-columns Hankel matrix $\mathbf{H}_{i,j}$ of impulse responses and their appropriate factorization. The first Hankel matrix is defined as [3]

$$\mathbf{H}_{i,j}=\begin{bmatrix}\mathbf{CB} & \mathbf{CAB} & \cdots & \mathbf{CA}^{j-1}\mathbf{B}\\ \mathbf{CAB} & \mathbf{CA}^{2}\mathbf{B} & \cdots & \mathbf{CA}^{j}\mathbf{B}\\ \vdots & \vdots & \ddots & \vdots\\ \mathbf{CA}^{i-1}\mathbf{B} & \mathbf{CA}^{i}\mathbf{B} & \cdots & \mathbf{CA}^{i+j-2}\mathbf{B}\end{bmatrix}=\mathbf{\Gamma}_i\mathbf{\Omega}_j, \tag{B.1}$$

where $\mathbf{\Gamma}_i$ is the $il\times n$ observability matrix described in Eq. (7) and $\mathbf{\Omega}_j=[\,\mathbf{B}\quad\mathbf{AB}\quad\cdots\quad\mathbf{A}^{j-1}\mathbf{B}\,]$ is the controllability matrix with dimension $n\times jm$. Two useful factorizations of matrix $\mathbf{H}_{i,j}$ can be derived, in terms of the system observability and controllability matrices as

$$\begin{aligned}\mathbf{H}_{1,j}&=\mathbf{\Gamma}_i^{(1)}\mathbf{\Omega}_j,\\ \mathbf{H}_{2,j}&=\mathbf{\Gamma}_i^{(2)}\mathbf{\Omega}_j=\mathbf{\Gamma}_i^{(1)}\mathbf{A}\mathbf{\Omega}_j.\end{aligned} \tag{B.2}$$

Matrix $\mathbf{H}_{i,j}$ can also be expressed in terms of individual elements of the scalar impulse response function,

$$h_{ij}(k)=\sum_{p=1}^{n} r_{ij(p)}\,\mathrm{e}^{\lambda_p\,\Delta t k}, \tag{B.3}$$

that is,

$$\begin{aligned}\mathbf{H}_{i,j}&=\begin{bmatrix}h_{ij}(1) & h_{ij}(2) & \cdots & h_{ij}(j)\\ h_{ij}(2) & h_{ij}(3) & \cdots & h_{ij}(j+1)\\ \vdots & \vdots & \ddots & \vdots\\ h_{ij}(i) & h_{ij}(i+1) & \cdots & h_{ij}(i+j-1)\end{bmatrix}\\ &=\begin{bmatrix}1 & \cdots & 1\\ z_1 & \cdots & z_n\\ \vdots & \ddots & \vdots\\ z_1^{i-1} & \cdots & z_n^{i-1}\end{bmatrix}\begin{bmatrix}r_{ij(1)} & & \\ & \ddots & \\ & & r_{ij(n)}\end{bmatrix}\begin{bmatrix}1 & z_1 & \cdots & z_1^{j-1}\\ \vdots & \vdots & \ddots & \vdots\\ 1 & z_n & \cdots & z_n^{j-1}\end{bmatrix}=\mathbf{\Pi}_i\mathbf{R}\mathbf{\Pi}_j,\end{aligned} \tag{B.4}$$

where $\mathbf{\Pi}_i$ has a Vandermonde structure comprised of terms $z_p^l=\left(\mathrm{e}^{\lambda_p\,\Delta t}\right)^l$. Matrix $\mathbf{H}_{i,j}$, described in terms of Vandermonde structure above, admits the following factorization:

$$\begin{aligned}\mathbf{H}_{1,j}&=\mathbf{\Pi}_i^{(1)}\mathbf{R}\mathbf{\Pi}_j,\\ \mathbf{H}_{2,j}&=\mathbf{\Pi}_i^{(2)}\mathbf{R}\mathbf{\Pi}_j=\mathbf{\Pi}_i^{(1)}\mathbf{Z}\mathbf{R}\mathbf{\Pi}_j,\end{aligned} \tag{B.5}$$

where $\mathbf{Z}=\mathrm{diag}\{\,z_1\quad\cdots\quad z_n\,\}$.

The state-vector transformation matrix $\mathbf{T}_d$ is obtained by making a connection between factorizations (B.2) and (B.5) for the single-input and single-output case as

$$\mathbf{H}_{2,j}=\mathbf{\Gamma}_i^{(1)}\mathbf{A}\mathbf{\Omega}_j=\mathbf{\Pi}_i^{(1)}\mathbf{Z}\mathbf{R}\mathbf{\Pi}_j \tag{B.6}$$

or equivalently,

$$\boldsymbol{\Gamma}_i^{(1)}\mathbf{A}\boldsymbol{\Omega}_j = \boldsymbol{\Pi}_i^{(1)}\left(\mathbf{T}_d\mathbf{T}_d^{-1}\right)\mathbf{Z}\left(\mathbf{T}_d\mathbf{T}_d^{-1}\right)\mathbf{R}\boldsymbol{\Pi}_j. \tag{B.7}$$

Imposing on the above equation the condition $\mathbf{A} = \mathbf{T}^{-1}\mathbf{Z}\mathbf{T}$ required in the particular realization described in Eq. (22), it follows immediately from above equation that

$$\boldsymbol{\Gamma}_i^{(1)} = \boldsymbol{\Pi}_i^{(1)}\mathbf{T}_d \tag{B.8}$$

or

$$\mathbf{T}_d = \boldsymbol{\Pi}_i^{(1)+}\boldsymbol{\Gamma}_i^{(1)}, \tag{B.9}$$

where + denotes the Moore–Penrose pseudo-inverse. Cambraia [10] shows that the transformation matrix $\mathbf{T}_d$ calculated as Eq. (B.9) is also valid for MISO case.

Eq. (B.9) shows the expression of matrix $\mathbf{T}_d$. In practice, the observability matrix $\boldsymbol{\Gamma}_i$ can be approximated by the extended observability matrix $\hat{\boldsymbol{\Gamma}}_i = \hat{\mathbf{Q}}_s$ as in Eq. (19) resulting in the following practical expression for $\mathbf{T}_d$ to be used for residues calculation

$$\mathbf{T}_d = \boldsymbol{\Pi}_j^{(1)+}\hat{\boldsymbol{\Gamma}}_i^{(1)} = \boldsymbol{\Pi}_j^{(1)+}\hat{\mathbf{Q}}_s^{(1)}, \tag{B.10}$$

where matrix $\boldsymbol{\Pi}_j$ is calculated from Eq. (B.4) using the identified poles and $\hat{\mathbf{Q}}_s$ is obtained from Eq. (18) for the MISO case according to the correspondent residues index $r_{ij(p)} = \phi_{i(p)}\phi_{j(p)}$.

## References


[1] N.M.M. Maia, J.M. Montalvão, J. He, N.A.J. Lieven, R.M. Lin, G.W. Skingle, W.M. To, A.P.V. Urtigueira, *Theoretical and Experimental Modal Analysis, Research Studies*, Wiley, New York, 1997.

[2] L. Ljung, *System Identification: Theory for the User*, Prentice-Hall, Englewood Cliffs, NJ, 1985.

[3] M. Viberg, Subspace-based methods for the identification of linear time-invariant systems, *Automatica* 31 (12) (1995) 1835–1851.

[4] B. Peeters, G. De Roech, Stochastic system identification for operational modal analysis: a review, *Journal of Dynamic System, Measurement and Control* 123 (2001) 659–667.

[5] L. Hermans, H. Van Der Auweraer, Modal testing of structures under operational conditions: industrial applications, *Mechanical System and Signal Processing* 13 (2) (1999) 193–216.

[6] L. Mevel, M. Basseville, M. Goursat, Stochastic subspace-based structural identification and damage detection—application to the steel-quake benchmark, *Mechanical System and Signal Processing* 17 (1) (2003) 91–101.

[7] M. Abdelghani, M. Goursat, T. Biochini, On line modal monitoring of aircraft structures under unknown excitation, *Mechanical System and Signal Processing* 13 (6) (1999) 839–853.

[8] J.N. Juang, System realization using information matrix, *Journal of Guidance, Control and Dynamics* 20 (3) (1997) 492–500.

[9] T. Kailath, *Linear System*, Prentice-Hall, Englewood Cliffs, NJ, 1980.

[10] H.N. Cambraia, Multivariable Subspace-Oriented Techniques Applied in Parameters Modal Identification, PhD Thesis, Universidade Estadual de Campinas, 2003.

[11] D.Z. Luo, A graphic explanation of undamped and damped mode shapes and its applications, *Journal of Sound and Vibration* 135 (3) (1989) 351–356.